



Investigation of Static Corrosion Between W Metals and TiN_x Barriers in a W Chemical-Mechanical-Polishing Slurry

Chi-Cheng Hung,^a Ying-Lang Wang,^{b,c,z} Wen-Hsi Lee,^{a,*} and Shih-Chieh Chang^b

^aDepartment of Electrical Engineering, National Cheng Kung University, Tainan 701, Taiwan

^bDepartment of Electrical Engineering, National Chia-yi University, Chia-yi, Taiwan

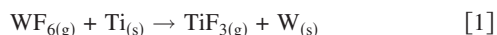
^cDepartment of Material Science, National University of Tainan, Tainan, Taiwan

In order to control the polishing qualities of tungsten (W) and titanium nitride (TiN_x) films in W chemical-mechanical-polishing (WCMP) processes, the electrochemical behavior between the W and the TiN_x films deposited at various N₂ flow rates was examined in this study. Metrologies, including X-ray diffractometry, Auger electron spectrometry, and scanning electron microscopy, were used to verify the physical properties of the TiN_x films, while electrochemical analyses, including electrochemical impedance spectroscopy, potential dynamic curves, and potential difference measurements, were used to characterize the mechanism of galvanic corrosion between the W and the TiN_x films deposited at various N₂ flow rates. The results show that the N content of the TiN_x films influences not only the physical properties of the TiN_x films but also the chemical activity in the WCMP slurries. The equivalent circuit, including the charge-transfer resistance and the titanium-oxide resistance associated with tantalum-oxide capacitance, was built to characterize the mechanism of the galvanic corrosion between the W and the TiN_x metals. © 2008 The Electrochemical Society. [DOI: 10.1149/1.2907394] All rights reserved.

Manuscript submitted December 30, 2007; revised manuscript received February 11, 2008.

Shrinking transistor sizes and the use of tall, three-dimensional capacitors in dynamic random access memory requires vertical interconnects (also called vias or plugs) in silicon integrated circuits.^{1,2} Chemical-vapor-deposited (CVD) tungsten (W) is the preferred method to realize the filling of a high-aspect-ratio contact via or plug due to its superior step-coverage.³⁻⁶ W is resistant to electromigration or stress migration due to its high melting point among pure metals (3387°C) and low resistivity (5.5 μΩ cm).

Prior to W deposition, titanium or its nitride (Ti/TiN_x) film is typically deposited as a glue layer because of the poor adhesion of W on SiO₂ substrates.⁷⁻¹¹ The TiN_x film further acts as a diffusion barrier, which offers protection against the reaction of tungsten hexafluoride (WF₆) and Ti, avoiding the W “volcano” effect. The volcano phenomenon occurs when WF₆ gas penetrates through the weak sites of TiN_x film and then rapidly reacts with the Ti underlayer, producing by-products of TiF₃ gas and solid W. The chemical formula for this reaction is as follows¹⁰



The TiN_x films are generally deposited using physical vapor deposition (PVD) or CVD. Conventional PVD-TiN_x films have been widely used as barrier layers because of their high chemical stability and low resistivity compared to CVD-TiN_x films. However, the step-coverage of the PVD process for high-aspect-ratio features is extremely difficult to achieve. A CVD-TiN_x film with a smaller overhang effect has been proposed as an alternative to the PVD-TiN_x film.^{12,13} After the glue layer and W deposition, overburdened metals are removed using W chemical-mechanical-polishing (WCMP) to define interconnects.^{14,15} WCMP is adopted for the redundancy of defective metal etching and better electrical yields to improve the overall integration for multilevel interconnects.¹⁶ However, the impact of a slurry attack and the influence of corrosion, including galvanic corrosion and intrinsic corrosion, during the WCMP process are significant.¹⁷⁻¹⁹ Galvanic corrosion is generated by the difference in the electrochemical potential at the interface between the W and the TiN_x metals in the slurry environment.

In this study, the galvanic effect between W and TiN_x metals in WCMP slurries is investigated. In order to improve the electrical properties of CVD-TiN_x films, an in situ plasma treatment using a hydrogen/nitrogen gas mixture is commonly employed to lower the level of C impurities and to form a crystallized TiN_x film.²⁰⁻²⁵ The

electrical properties of CVD-TiN_x films are highly plasma-treatment sensitive. The physical and chemical properties of the TiN_x films are dependent on the plasma treatment conditions due to different N/Ti ratios of the TiN_x films. In order to verify the galvanic effect between the W and the TiN_x films with different nitrogen content, PVD-TiN_x films with N/Ti ratios controlled by various nitrogen (N₂) gas-flow rates are investigated with W metals using electrochemical analyses. The results demonstrate that nitrogen content is critical in the formation of titanium-metal oxidation and the galvanic corrosion between the W and the TiN_x films. In order to obtain a robust W metallization process, the N content of the TiN_x barriers should be optimized to achieve a compromise between the barrier properties and chemical stability.

Experimental

In this study, blanket wafers were deposited with 50 nm thick TiN_x films using the PVD process and 100 nm thick W films using the CVD process on 300 nm SiO₂/Si(100) substrates. The base pressure of the PVD system was ~4 × 10⁻⁶ Torr. The TiN_x barriers were deposited from a Ti target (99.9995%). The Ar flow was kept at 25 sccm, while the nitrogen flow was varied from 20 to 80 sccm, resulting in a process pressure of ~0.2 Torr. The gas purity was 99.9999%. The gas-flow rate was controlled to within ±0.1 sccm by mass-flow controllers, which guaranteed reproducible deposition conditions. In the WCVD process, the nucleation W layer was deposited using WF₆ and SiH₄ precursors at 395°C. The bulk-W film was then in situ deposited using the H₂ reduction of WF₆ at 395°C in the same chamber.

In the corrosion analyses, the TiN_x films deposited at various N₂ flow rates were used as the working electrodes (4 cm²), W plug films were used as the counter electrodes (4 cm²), and Ag/AgCl was used as a reference electrode in a WCMP slurry, which contained aluminum oxide abrasive, surfactant, and hydrogen peroxide (~5% H₂O₂) with a pH of 2–3. The Nyquist plot was measured using a Princeton Applied Research PARSTAT 2273 to analyze the ac impedance behavior of the capacitor cells. The impedance measurements were carried out at various potential values with a dc potential amplitude of 0 mV, associated with open-circuit potential, and a frequency range of 10 mHz to 1000 kHz. The equivalent circuit was built and simulated using ZSimpWin version 3.1 with electrical impedance spectroscopy (EIS) data. The potential difference between the W and the TiN_x metals was measured by electrically connecting two electrodes to an electrometer, which is a high-impedance multimeter that can measure electrical voltages, resistance, and current. The N content of the PVD-TiN_x films was deter-

* Electrochemical Society Active Member.

^z E-mail: ylwang@tsmc.com

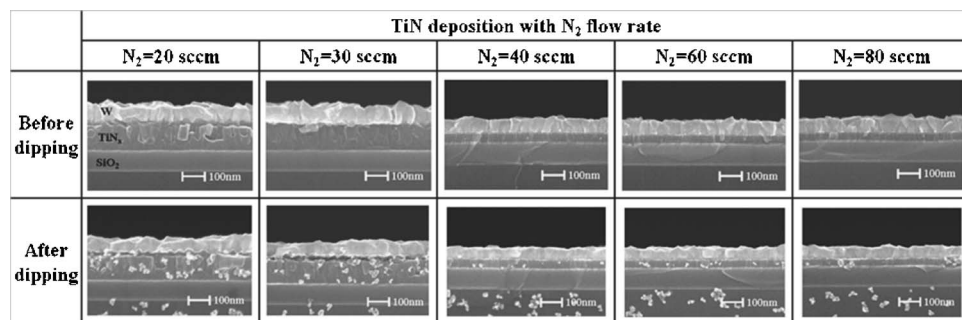


Figure 1. Cross-sectional SEM images (before and after dipping) of W plugs and TiN_x films deposited at various N_2 flow rates.

mined using an Auger electron spectrometer, which used a 10 kV E-beam and a 3 kV ion gun, with an ion gun sputter rate of 2.19 \AA/s . The O ratio of TiN_x films after dipping was obtained using energy-dispersive X-ray (EDX). The texture of the TiN_x films was identified using X-ray diffractometry (XRD) with Cu $\text{K}\alpha$ radiation (wavelength of 1.54 \AA) at 40 kV and 50 mA. The cross-sectional profile and the thickness of the TiN_x/W films before and after slurry dipping were reviewed using a field-emission scanning electron microscope (SEM) of the KLA-Tencor SEMVision tool.

Results and Discussion

Figure 1 shows cross-sectional SEM images (before and after slurry dipping) of the W and the TiN_x films deposited at the N_2 flow rates from 20 to 80 sccm. The thicknesses and structures of the TiN_x films clearly change with the N_2 flow rate. The relationship of the N stoichiometry and the deposition rates of PVD- TiN_x films with various N_2 flow rates is shown in Fig. 2. The N stoichiometry increases with increasing N_2 flow rate, while the deposition rate of the PVD- TiN_x films decreases with increasing N_2 flow rate. Increasing the amount of N_2 gas in the chamber during the TiN_x deposition increased the number of Ti-N compounds that were formed on the Ti target, resulting in a higher target resistance. The poison effect reduces the efficiency of the plasma bombardment to the target and decreases the deposition rate of the PVD- TiN_x films.^{17,18} The increased formation of the Ti-N compounds also caused an increase in the N stoichiometry of the PVD- TiN_x films. In the corrosion analysis, the corrosion thickness is the difference between the film (W or TiN_x) thickness before and after slurry dipping. The corrosion thickness of the W and the TiN_x films deposited at N_2 gas-flow rates from 20 to 80 sccm after dipping the W/ TiN_x bilayer films in the WCMP slurry is shown in Fig. 3. The corrosion of bilayer films in the chemical-mechanical-polishing (CMP) slurry includes self-corrosion and galvanic corrosion.¹⁷ The self-corrosion means that the film (W

or TiN_x) corrodes in the slurry. Galvanic corrosion results from the potential difference between W metal and TiN_x films in the WCMP slurry.

When the N_2 gas-flow rate increased from 20 to 40 sccm, the corrosion thickness of the TiN_x films decreased from ~ 5 to $\sim 2.1 \text{ nm}$. A further increase in the N_2 gas-flow rate, from 40 to 80 sccm, led to an increase in the corrosion thickness of the TiN_x films. However, the corrosion thickness of the W films increased with increasing N_2 gas-flow rate. Figure 4 shows the potential dynamic curves of the W and the TiN_x metals obtained from measurements using Princeton Applied Research PARSTAT 2273. It was found that the corrosion current density (I_{corr}) of the W metal is much higher than that of the TiN_x films, implying that the intrinsic corrosion rate of the W metals is much higher than that of the TiN_x films.

When the N_2 gas-flow rate increased from 20 to 40 sccm, the TiN_x films were less active than W metals in the WCMP slurry. When the N_2 gas-flow rate was larger than 40 sccm, the W films were less active than the TiN_x films in the WCMP slurry. Therefore, the potential difference between the W metals and the TiN_x films deposited at N_2 gas-flow rates from 20 to 80 sccm measured using an electrometer can be naturally divided into two groups, as seen in Fig. 5. One group is the positive potential difference. The simple oxidation half reactions of the W and Ti metals are shown as Eq. 2 and 3, respectively



From the electrochemical reactions, the relationship of galvanic corrosion between the W and the TiN_x metals is as shown in Eq. 4

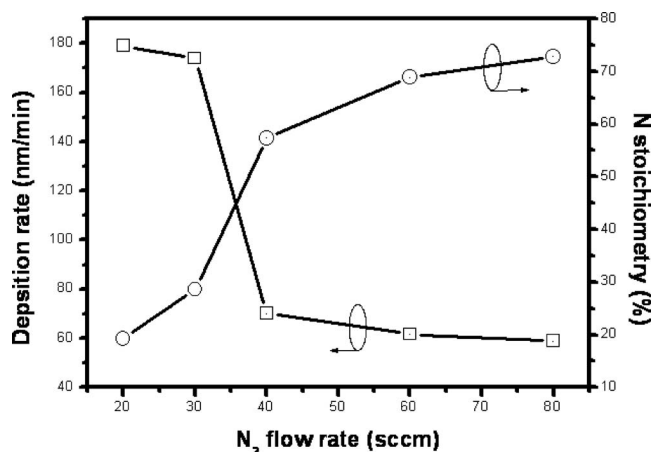


Figure 2. Relationship of N element ratio and deposition rates of PVD- TiN_x films at various N_2 flow rates.

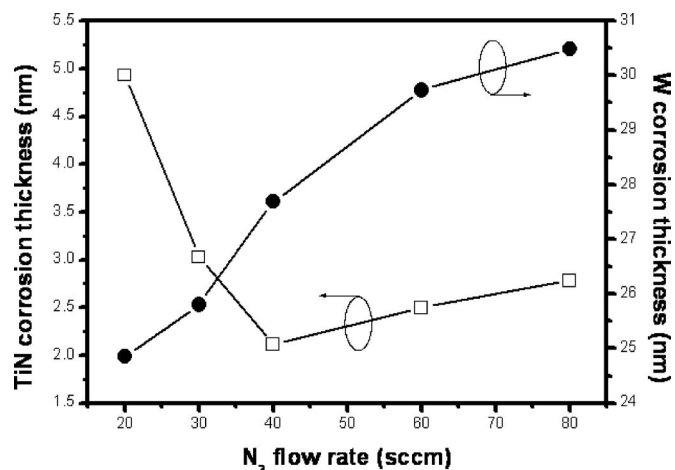


Figure 3. Corrosion thickness of the W plugs and the TiN_x films deposited at various N_2 gas-flow rates after slurry dipping.

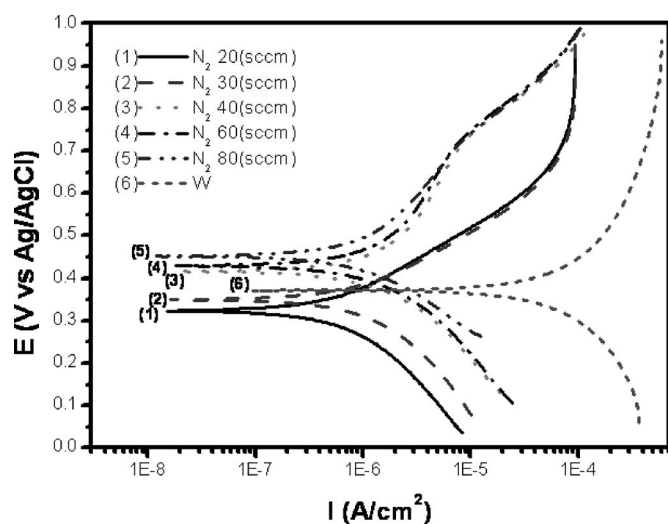


Figure 4. Potential dynamic curves of the W plugs and the TiN_x films deposited at various N_2 gas-flow rates in the slurries.

$$W_{\text{Corr}} \sim \mu \cdot \text{Ti}_{\text{Corr}} \quad [4]$$

where $\mu = 2M_{\text{W}}D_{\text{Ti}}/3M_{\text{Ti}}D_{\text{W}} \approx 0.6$, in which M_{W} is the molecular weight of W ≈ 183.92 g/mol, M_{Ti} is the molecular weight of Ti ≈ 47.9 g/mol, D_{W} is the density of W ≈ 19.3 g/cm³, and D_{Ti} is the density of Ti ≈ 4.54 g/cm³. The other group is the negative potential difference. The oxidation half reactions of the W and Ti metals are the opposite of those above, resulting from the TiN_x films being nobler, as seen in Eq. 5 and 6

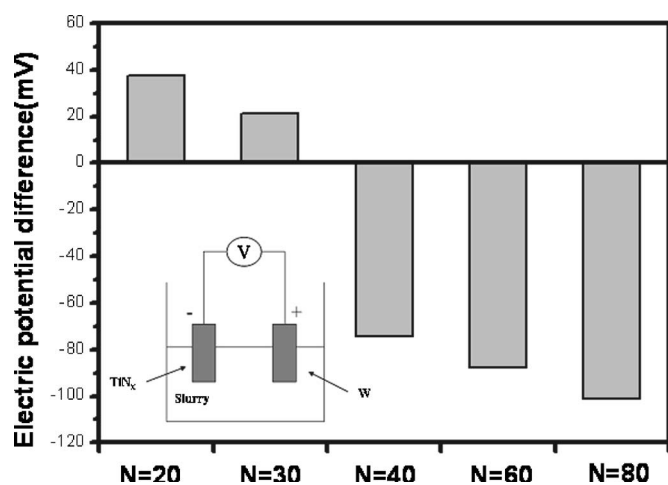
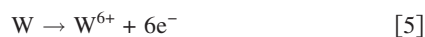


Figure 5. Potential difference between the W plugs and the TiN_x films deposited at various N_2 gas-flow rates from 20 to 80 sccm.

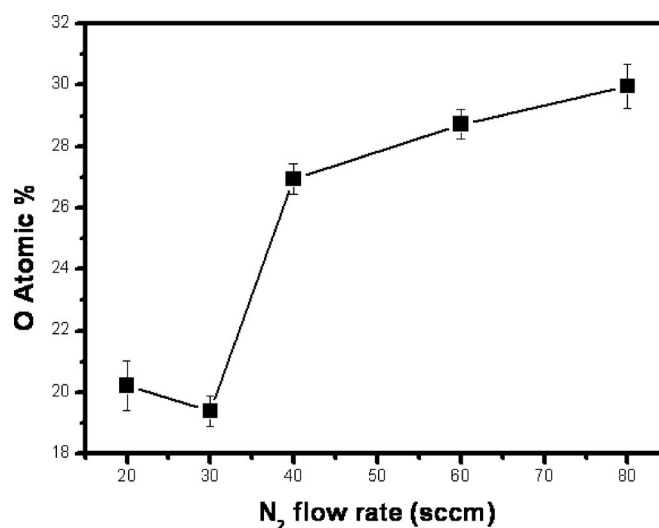


Figure 6. EDX of the O element ratio of the TiN_x films deposited at various N_2 gas-flow rates after slurry dipping.



The relationship of galvanic corrosion between the W and the TiN_x films is as shown in Eq. 7

$$\text{Ti}_{\text{Corr}} \sim v \cdot W_{\text{Corr}} \quad [7]$$

where $v = 1.5M_{\text{W}}D_{\text{Ti}}/M_{\text{Ti}}D_{\text{W}} \approx 1.66$. Table I shows the galvanic and intrinsic corrosion rates of the W and the TiN_x films. The results are consistent with Eq. 4 and 7.

Figure 6 shows the O element content of TiN_x films deposited at various N_2 flow rates. It demonstrates that the oxidation of TiN_x films is influenced by N doping, which is proven by the intrinsic corrosion rates of the TiN_x films, as shown in Table I.

Figure 7 shows the XRD patterns for the texture evolution of the as-deposited TiN_x films with N_2 flow rates from 20 to 80 sccm. When the N_2 flow rate increases from 20 to 30 sccm, the tetragonal Ti_2N , the face-centered cubic TiN, and the Ti phase of the TiN_x films gradually disappear. After a further increase in the N_2 flow rate from 30 to 80 sccm, the phase of TiN_x almost completely transforms into an amorphous phase. This is probably due to the formation of an amorphous nitrogen-rich film. The change of the TiN_x phase also demonstrates that the TiN_x films are nobler than the W metals in the WCMP slurry when the N_2 gas-flow rate is larger than 40 sccm.

The Bode plots of Fig. 8a show the effect of applied frequency on the corrosion impedance between the W metals and the TiN_x films deposited at N_2 gas-flow rates from 20 to 80 sccm. TiN_x films deposited at various N_2 flow rates were used as the working electrodes, W films were used as the counter electrodes, and all potentials were measured relative to the Ag/AgCl reference electrodes. In the high-frequency region (>100 kHz), which is the inset of Fig.

Table I. Summary of intrinsic and galvanic corrosion between W plug and TiN_x films deposited with various N_2 flow rates. Units are in nm/min.

	TiN self-corrosion rate	TiN galvanic corrosion rate	W self-corrosion rate	W galvanic corrosion rate
$\text{N}_2 = 20$ sccm	0.934	0.711	8.668	-0.385 ^a
$\text{N}_2 = 30$ sccm	0.926	0.084	8.647	-0.046
$\text{N}_2 = 40$ sccm	2.356	-1.651	8.512	0.717
$\text{N}_2 = 60$ sccm	2.823	-1.989	8.737	1.175
$\text{N}_2 = 80$ sccm	3.311	-2.383	8.521	1.642

^a Minus (-) means that TiN/W reduction occurs during galvanic corrosion.

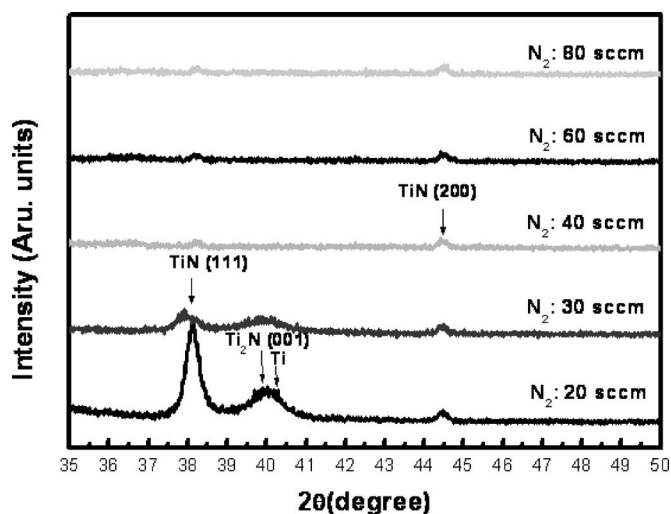
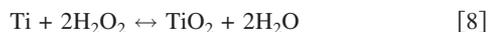


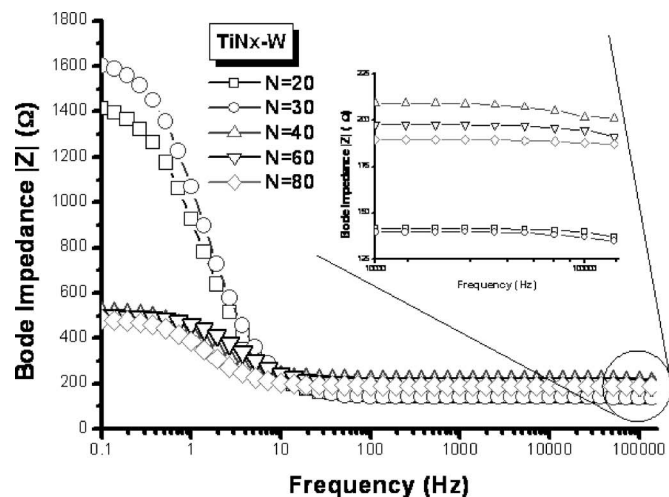
Figure 7. XRD patterns of IMP-TiN_x films deposited at various N₂ flow rates.

8a, the impedance is divided into two groups. The impedance indicates the same trend for the measurements in the low-frequency region (0.01–0.1 Hz), as shown in Fig. 8a. Figure 8b shows Nyquist plots of the TiN_x-W electrochemical system in the CMP slurry. Z_{im} is the imaginary resistance and Z_{re} is the real resistance. The simulated equivalent circuit of the TiN_x-W electrochemical system, which is the inset of Fig. 8b, was built according to the method used in our previous reference. In this circuit, R_s is the bulk-solution resistance, C_{dl} is the double-layer capacitance of the electricity generated from surface corrosion of the TiN_x films, C_{ox} is the capacitance of the TiN_x oxidation layer in the form of constant phase element (CPE), R_{corr} is the charge-transfer resistance (associated with the double layer), and R_{ox} is the resistance of the TiN_x oxidation layer.¹⁸ Furthermore, R_{ox} and R_{corr} are in parallel, because surface oxidation and corrosion of the TiN_x films occur at the same time in the TiN_x-W electrochemical system. Two semicircles respectively express the transient surface oxidation of the TiN_x films, as shown in Fig. 8b and c, which is a magnification of the impedance close to zero in the high-frequency region (> 100 kHz). The chemical reaction of the TiN_x films in the presence of hydrogen peroxide proceeds in the following intermediate steps

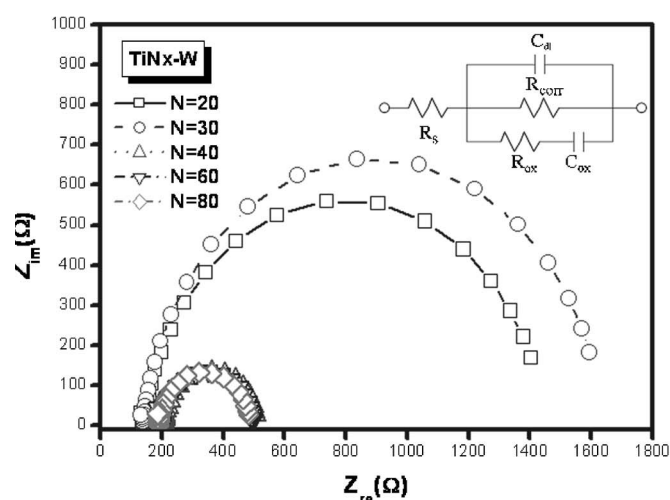


Hence, the first semicircle (Fig. 8c) shows the high-frequency region and indicates that the Ti metal oxidizes in peroxide-based solutions (Eq. 8), and the second semicircle (Fig. 8b) shows the low-frequency region and indicates the continuous corrosion of the TiN_x films (Eq. 9).

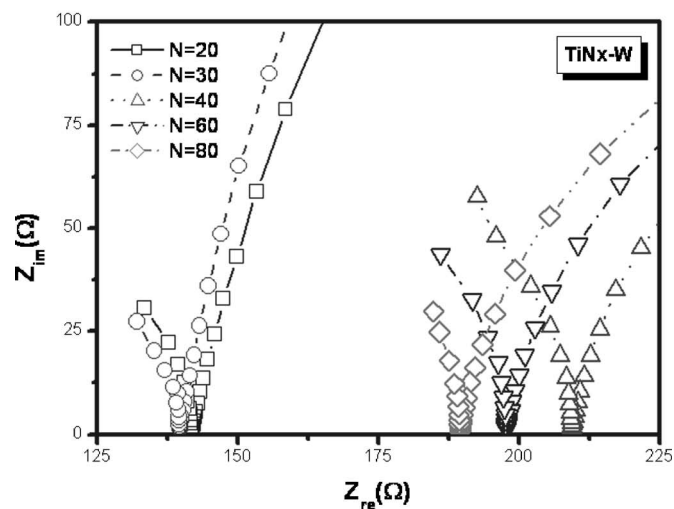
When the N₂ flow rate is in the range of 20–30 sccm, the TiN_x film acts as an anode (Eq. 2) compared to the W metal in the TiN_x-W electrochemical system. The potential difference between the TiN_x and W films is smaller and decreases with increasing N₂ flow rate. Therefore, the galvanic corrosion of the TiN_x films and the formation of TiO₂ enhanced by the W metal are slight and tend to be suppressed. The values of circuit components were obtained by fitting the Nyquist spectra of Fig. 8b and are summarized in Table II. According to our earlier study, the elements of the circuit, including R_{ox} , C_{ox} , and R_{corr} , help explain the mechanism of the oxidation and corrosion of the TiN_x films.¹⁸ The tendencies of R_{ox} , C_{ox} , and R_{corr}



(a)



(b)



(c)

Figure 8. (a) Bode plots [the inset is a magnification of the high-frequency region (> 100 kHz)], (b) Nyquist plots of the W plugs and the TiN_x films at N₂ flow rates from 20 to 80 sccm, and (c) a magnification of impedance close to zero in the high-frequency region.

Table II. Element value of equivalent circuit required for best fitting of impedance spectra in Fig. 8b.

TiN _x -W	R _s (Ω)	R _{ox} (Ω)	CPE _{ox}		C _{ox} (μF)	R _{corr} (Ω)	C _{dl} (nF)
			Y _{ox} (μΩ ⁻¹)	α _{ox}			
N = 20	24.26	128.1	255.9	0.9058	179.35	1429	2.715
N = 30	25.84	122.4	264.1	0.9235	198.75	1615	2.875
N = 40	25.28	295.5	168.4	0.9312	134.92	489.2	2.276
N = 60	24.27	273.4	194.7	0.9296	155.92	474.9	1.778
N = 80	24.02	257.5	208.9	0.9323	168.95	463.4	1.371

verify that the formation of TiO₂ and the galvanic corrosion of the TiN_x films decrease with increasing N₂ flow rate because nitrogen inhibits the electron release from the TiN_x film to the W film, as shown in Table II. The galvanic corrosion rate of the TiN_x films, shown in Table I, is consistent with the results of Fig. 8b. The C_{dl} value, corresponding to the generation of electrons, becomes smaller, resulting from the reduction of I_{corr}.

After a further increase of the N₂ flow rate in the range of 40–80 sccm, the TiN_x film acts as a cathode (Eq. 6) compared to the W metals in the TiN_x-W electrochemical system. The potential difference between the TiN_x and W films is larger and increases with increasing N₂ flow rate; therefore, the galvanic corrosion of the TiN_x films is faster and tends to accelerate. Because of the increasing reduction of Ti⁴⁺ ions to Ti metal, the formation of TiO₂ reduces because it accelerates corrosion to replenish Ti⁴⁺ ions (Eq. 9). Similarly, the increase of C_{ox} and the decrease of R_{ox} and R_{corr} verify the reduction of the TiO₂ thickness and the increase in the corrosion rate of the TiN_x films with increasing N₂ flow rate, as shown in Table II. Therefore, the elements of the circuit in the TiN_x-W electrochemical system represent their physical meanings. Using the parameters of impedance spectroscopy, the mechanism of the galvanic corrosion between the W metals and the TiN_x barriers can be investigated.

Conclusions

In conclusion, the N content of the TiN_x films affected not only the physical film properties but also the chemical activity in the WCMP process. The mechanism of galvanic corrosion in the TiN_x-W electrochemical system was investigated. An equivalent circuit simulated using EIS data was built to characterize the surface reaction between the W metals and the TiN_x films. With an increasing N₂ flow rate in the PVD-TiN_x process, the potential difference between the W metals and the TiN_x films in the WCMP slurry changes to negative from positive, while the role of the TiN_x film changes to a cathode from an anode. The results demonstrate that the N element content affects the formation of titanium-metal oxidation and the galvanic corrosion between the W metals and the TiN_x films. In order to have a robust W metallization process, the N content of the TiN_x barriers should be optimized to achieve a compromise between the barrier properties and chemical stability.

Acknowledgment

This work was supported by the National Science Council of Taiwan (grant no. NSC 96-221-E-006-125 and NSC 97-2623-7-006-012-ET). The authors thank the National Cheng Kung University, Tainan, Taiwan for its technical support.

National Chen Kung University assisted in meeting the publication costs of this article.

References

1. T. Kaga, M. Ohkura, F. Murai, N. Yokoyama, and E. Takeda, *J. Vac. Sci. Technol. B*, **13**, 2329 (1995).
2. S. B. Herner, S. A. Desai, A. Mak, and S. G. Ghanayem, *Electrochem. Solid-State Lett.*, **2**, 398 (1999).
3. A. C. Westerheim, J. M. Bulger, C. S. Whelan, T. S. Sriram, L. J. Elliott, and J. J. Maziarz, *J. Vac. Sci. Technol. B*, **16**, 2729 (1998).
4. C. Faltermeier, C. Goldberg, M. Jones, A. Upham, D. Manger, G. Peterson, J. Lau, and A. Kaloyeros, *J. Electrochem. Soc.*, **144**, 1002 (1997).
5. P. J. Ireland, *Thin Solid Films*, **304**, 1 (1997).
6. H. L. Chang and P. R. Jeng, *Jpn. J. Appl. Phys., Part 1*, **39**, 4378 (2000).
7. S. Parikh, L. Akselrod, J. Gardner, K. Armstrong, and N. Parekh, *Thin Solid Films*, **320**, 26 (1998).
8. J. Wu, Y. L. Wang, J. Dun, Y. L. Wu, H. Zhang, and A. Wang, *J. Vac. Sci. Technol. B*, **17**, 2300 (1999).
9. S. B. Herner, Y. Tanaka, H. Zhang, and S. G. Ghanayem, *J. Electrochem. Soc.*, **147**, 1982 (2000).
10. H. L. Chang, F. L. Juang, and C. T. Kuo, *Jpn. J. Appl. Phys., Part 1*, **41**, 2906 (2002).
11. S. H. Kim, E. S. Hwang, S. Y. Han, S. H. Pyi, N. Kawk, H. Sohn, J. Kim, and G. B. Choi, *Electrochem. Solid-State Lett.*, **7**, G195 (2004).
12. Y. Nakasaki, K. Suguro, and M. Kashiwagi, *J. Appl. Phys.*, **64**, 3263 (1988).
13. P. Dekker, P. J. Van der Put, H. J. Veringa, and J. Schoonman, *J. Electrochem. Soc.*, **141**, 787 (1994).
14. C. Yu, S. Poon, Y. Limb, T. K. Yu, and J. Klein, in *Proceedings of the VLSI Multilevel Interconnection Conference*, Santa Clara, CA, p. 144 (1994).
15. M. Rutton, P. Feeney, R. Cheek, and W. Landers, in *Proceedings of the VLSI Multilevel Interconnection Conference*, Santa Clara, CA, p. 491 (1995).
16. J. Lee, J. Kim, and H. Shin, *Thin Solid Films*, **320**, 15 (1998).
17. C. C. Hung, Y. S. Wang, W. H. Lee, S. C. Chang, and Y. L. Wang, *Electrochem. Solid-State Lett.*, **10**, H127 (2007).
18. C. C. Hung, W. H. Lee, Y. S. Wang, S. C. Chang, and Y. L. Wang, *Electrochem. Solid-State Lett.*, **10**, D100 (2007).
19. S. Kondo, N. Sakuma, Y. Homma, and N. Ohashi, *Jpn. J. Appl. Phys., Part 1*, **39**, 6216 (2000).
20. R. Kröger, M. Eizenberg, C. Marcadal, and L. Chen, *J. Appl. Phys.*, **91**, 5149 (2002).
21. S. Ikeda, J. Palleau, J. Torres, B. Chenevier, N. Bourhila, and R. Madar, *J. Appl. Phys.*, **86**, 2300 (1999).
22. S. Ikeda, J. Palleau, J. Torres, B. Chenevier, N. Bourhila, and R. Madar, *Solid-State Electron.*, **43**, 1063 (1999).
23. D. H. Kim and B. Y. Kim, *Jpn. J. Appl. Phys., Part 2*, **38**, L461 (1999).
24. S. H. Whang, J. K. Kim, J. W. Park, D. H. Kim, D. L. Cho, and W. J. Lee, *Jpn. J. Appl. Phys., Part 1*, **40**, 265 (2001).
25. B. K. Lim, H. S. Park, A. K. H. See, E. Z. Liu, and S. H. Wu, *J. Vac. Sci. Technol. B*, **20**, 2219 (2002).